LEAKAGE FLOW NOISE AND RELATED FLOW PATTERN IN A LOW-SPEED AXIAL FAN WITH ROTATING SHROUD

E. Canepa, A. Cattanei, F. Mazzocut Zecchin

DIME-Università di Genova, via Montallegro, 1, I-16145 Genova, Italy

ABSTRACT

The effect of rotational speed and pressure rise on the leakage flow noise radiated by a low-speed axial fan, provided with rotating shroud, has been systematically investigated. The leakage flow noise generally increases with the blade loading, with a trend which is qualitatively independent from the rotational speed but non-monotonic, as its growth is interrupted by local minima. As the loading increases, the SPL spectrum shows important modifications, since the characteristic frequency of the subharmonic narrowband humps related to the leakage noise decreases. The flow in the gap region has been studied by means of PIV measurements taken in the meridional plane. At low blade loading, the leakage flow is restrained close to the rotor ring and, at higher loading, it forms a wide recirculation zone. In the latter conditions, an unsteady flow separation likely takes place in the blade tip region which may be observed in the instantaneous flow field only. Possibly, it is responsible for the observed frequency shift of the humps.

KEYWORDS

LEAKAGE FLOW, FAN NOISE, AXIAL-FLOW FAN, PIV

NOMENCLATURE

c	blade chord
f	frequency
G	acoustic propagation function
OASPL	overall SPL, ref. 20 μPa
p	acoustic pressure
Q	volume flow rate
r	radial coordinate
Re_c	Reynolds number based on blade chord and relative velocity w
S_{pp}	one-sided auto power spectral density of p
SPL	sound pressure level in a given frequency band (SPL spectrum), ref. 20 μPa
St	Strouhal number based on the rotational frequency, $60f/\Omega$
Tu	turbulence intensity based on u_{tip}
u_{tip}	peripheral speed of the blade
v_a, v_r, v_θ	components of the absolute velocity
α	scaling exponent
Δp	pressure rise through the rotor (static outlet minus total inlet)
ρ_0	air density
φ	flow coefficient, $\frac{Q}{u_{tip}\pi {r_{tip}}^2}$
ψ	pressure rise coefficient, $\frac{\Delta p}{0.5\rho_0 {u_{tip}}^2}$
Ω	rotational speed (expressed in rev/min)

Superscripts

OPEN ACCESS
Downloaded from www.euroturbo.eu

Copyright © by the Authors

$\tilde{}$ related to the ensemble average
$\bar{}$ related to the time average
$'$ related to non-periodic instantaneous fluctuations

Subscripts

DP related to design operating conditions
filt related to the filtered SPL, Eq. (3)
high related to the range 300 > *St* > 90
hub related to the rotor hub
low related to the range 6 < *St* < 90
scaled related to the scaled SPL, Eq. (1)
tip related to the blade tip

INTRODUCTION

The axial fans employed in automotive cooling systems are commonly provided with a rotating shroud, i.e. a ring connecting the blade tips. This ring improves the volumetric efficiency and also strengthens the whole assembly, but it often increases the radiated noise, due to the presence of large-scale turbulent structures. They are contained in the leakage flow released from the gap between the rotating ring and the stationary enclosure and are eventually reingested by the rotor. Their interaction with the rotor blades results in noise in the low- to medium-frequency range, with the appearance of narrowband humps at subharmonic frequencies and a general increase of the broadband noise. The leakage flow noise often constitutes the major contribution to the overall radiation and its main features are known, but very few works related to it are available in the literature, e.g. see Fukano et al. (1986), Fukano and Jang (2004), Piellard et al. (2014), Magne et al. (2015), Moreau and Sanjose (2016), Zenger et al. (2016), Na et al. (2017), Canepa et al. (2016a, 2018, and 2019) and Zhu et al. (2018). In order to find effective solutions for noise reduction, a deeper insight in the leakage flow features and in the effect of relevant parameters is necessary. The present paper continues the aerodynamic and acoustic investigation reported in Canepa et al. (2018 and 2019), which was conducted on a plastic rotor employed in real cooling units. That research showed that different patterns may exist for the leakage flow, which also affect the radiated noise. Beyond an obvious dependence of such patterns on gap geometry and on operating conditions, an unexpected dependence on both rotational speed and pressure rise was also observed, due to the related rotor deformation. This raised a number of questions on the features of the phenomenon and also on the validity of the acoustic similarity, see Neise and Barsikow (1982) or Canepa et al. (2017), which allows scaling the results of acoustic measurements related to different rotational speeds. Hence, it has been decided to perform a more systematic investigation on an aluminum rotor, which may be considered stiff. The larger number of investigated operating conditions and rotational speeds provide a more complete picture of the phenomenon.

EXPERIMENTAL PROCEDURE

Experimental facility

Compared to the previous works, see Canepa et al. (2016a, 2017, 2018, 2019), in the present study, a larger number of operating conditions have been investigated, and a different rotor has been tested, see Fig. 1. It also has 9 blades of different geometry and is an aluminum prototype. The previously studied rotor is a plastic one employed in a real cooling unit. Opposite to the latter, the former rotor may be considered stiff. It has a tip radius r_{tip} = 222 mm, a hub-to-tip diameter ratio r_{hub}/r_{tip} = 0.374, and a chord c which varies between 43 mm and 50 mm from hub to tip. At the design point, the flow coefficient is $\varphi_{DP} = \frac{Q_{DP}}{u_{tip}\pi {r_{tip}}^2} = 0.0869$ and the pressure rise coefficient is $\psi_{DP} = \frac{\Delta p_{DP}}{0.5\rho_0 {u_{tip}}^2} = 0.0993$, with Δp the fan pressure rise (outlet static pressure minus inlet total one).

For the previously studied rotor, r_{tip} = 227 mm, r_{hub}/r_{tip} = 0.391, φ_{DP} = 0.098, and ψ_{DP} = 0.12. Both rotors have been mounted on a test plenum (TP) designed according to ISO standards (1996). The TP has a limited interaction with acoustic waves and allows varying the operating point simply acting on the width of the TP back slot (BS), see Fig. 1a. The non-dimensional characteristic curve of the rotor of Fig. 1d has been obtained from measurements taken at Ω = 2000 and 2500 rev/min. The good collapse of the two sets of points shows that overall aerodynamic similarity holds above 2000 rev/min at least. Hence, constancy of any of φ or ψ guaranties that similarity is respected. Under the realistic assumption that the pressure drop through the BS is proportional to Q^2, the rotor is expected to work at fixed operating point if the BS width is kept unchanged while Ω varies. During the tests, the pressure inside the TP has been measured and the ψ trend has been controlled.

Acoustic measurement procedure and data processing technique

Acoustic measurements have been taken in the DIME anechoic chamber with a B&K 3560 spectrum analyzer and a ½" free-field microphone with the microphone mounted on-axis 1 m

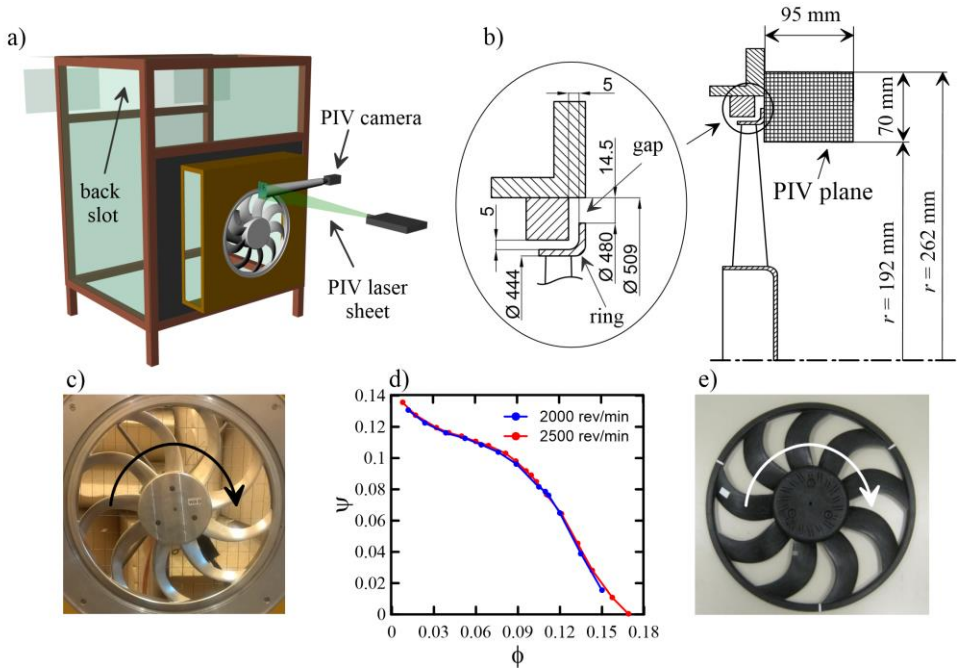

Figure 1: Experimental facility. a) Test plenum. b) PIV measurement domain and gap geometry (not to scale). c) Investigated rotor. d) Non-dimensionalized characteristic curves of the rotor. e) Previously studied rotor.

upstream of the rotor. Due to the low-frequency loss of anechoicity of the chamber, the part of the spectra below 100 Hz are blanked in the plots. The tests have been done in the range Ω = 1000 ÷ 4000 rev/min at Ω = *const* and during low-angular-acceleration linear Ω ramps (3000 rev/min variation within 1080 s), for a total amount of 13 ψ values which include the four conditions at which aerodynamic measurements have been taken. At Ω = 2500 rev/min, the reference Reynolds number $Re_c = wc/\nu$ varies from 32500 to 43300 at the rotor hub and from 194000 to 196000 at the blade tip.

Constancy of ψ during a speed ramp should imply that, beyond aerodynamic similarity, the aeroacoustic one is respected also, e.g. see Neise and Barsikow (1982) or Canepa et al. (2017). However, noise generation may be strongly affected by flow details which do not apparently affect the φ-ψ characteristic curve, and hence a preliminary analysis of the SPL spectra is required. As for the leakage flow noise, attention has to be focused on the low-frequency part of the sound pressure level (SPL) spectrum. A first check may consist in the analysis of SPL_{low}, that is the SPL in the range $St = 6 \div 90$, $St = 60f/\Omega$ being the Strouhal number. SPL_{low} strongly increases with Ω and scaling it with $10\log_{10}\Omega^{4+\alpha}$ allows eliminating the gross dependence:

$$\mathrm{SPL}_{\mathrm{low,scaled}}(\Omega,\psi) = \mathrm{SPL}_{\mathrm{low}}(\Omega,\psi) - 10\log_{10}\Omega^{4+\alpha} \quad (1)$$

α is an exponent close to 1 to be tuned case by case. Further information on the noise generating mechanisms are provided by the high frequency part of the SPL spectrum, $\mathrm{SPL}_{\mathrm{high}}$, ($St = 90 \div 300$) and by the overall SPL ($St = 6 \div 300$), OASPL. Given that $S_{pp}(f, \Omega, \psi)$ is the one-sided power spectral density of the received acoustic pressure, the SPL in the frequency band $f_{min} \div f_{max}$ is given by

$$\mathrm{SPL}(f,\Omega,\psi) = 10\log_{10}\left[\frac{1}{p_{ref}^2}\int_{f_{min}}^{f_{max}} S_{pp}(f,\Omega,\psi)\mathrm{d}f\right] \quad (2)$$

where $p_{ref} = 20$ μPa is the reference pressure and $f = (f_{min} + f_{max})/2$ is the central frequency of the band. If the bandwidth $\Delta f = f_{max} - f_{min}$ is small enough (typically less than 20 Hz), the sequence $\mathrm{SPL}_n = \mathrm{SPL}(f_n)$ with $f_n = n\Delta f$ constitutes the SPL spectrum.

In the computation of $\mathrm{SPL}_{\mathrm{low}}$ and $\mathrm{SPL}_{\mathrm{high}}$, f_{min} and f_{max} are obtained substituting the related *St* values in the relation $f = \Omega\, St/60$. If aeroacoustic similarity holds, $\mathrm{SPL}_{\mathrm{low,scaled}}$ and $\mathrm{SPL}_{\mathrm{high,scaled}}$ show a linear dependence on Ω and are constant if the actual α value is employed. As for the SPL spectra, the characteristic frequencies should scale with Ω if the rotor is operated under aerodynamic similarity. Namely, S_{pp} features such as peaks, humps, dips, etc. should be characterized by the same *St* as Ω varies, resulting in vertical stripes in a *St*-Ω spectrogram as the one of Fig. 2b. In fact, for a given rotor and test-rig mounted in an anechoic chamber, acoustic propagation effects such as diffraction or resonance are independent from the noise generating mechanism and, hence, from Ω. They may affect different parts of the SPL spectrum if measurements are repeated at different Ω, e.g. see Canepa et al. (2017), and should be eliminated as they complicate analyzing the SPL spectra. If *St* is fixed, SPL oscillations superposed to a growing trend typically result. On the contrary, quantities such as $\mathrm{SPL}_{\mathrm{low}}$ and $\mathrm{SPL}_{\mathrm{high}}$ are usually less affected due to the large frequency ranges they are related to. In the present configuration, such effects consist in a number of dips due to the mounting panel (at $f = 150$, 500, and 1250 Hz) and in oscillations due to the TP in the range $f = 1900 \div 3500$ Hz, see Canepa et al. (2015 and 2016a). In a *St*-Ω spectrogram, propagation effects typically appear as crests and valleys aligned along hyperbolas, e.g. see Fig. 2b. In order to eliminate them, the method presented by Bongiovì and Cattanei (2011) has been employed. Such a method allows to compute the propagation function $G(f)$, which contains the propagation effects and is then subtracted from the SPL spectrum, e.g. see Fig. 3c. This results in the so called filtered SPL:

$$\mathrm{SPL}_{filt}(f,\Omega,\psi) = \mathrm{SPL}(f,\Omega,\psi) - 20\log_{10}G(f) \quad (3)$$

Aerodynamic measurement procedure and data processing technique

The flow field in the meridional plane close to the tip gap, see Fig. 1b, has been investigated in a 70 mm × 95 mm (radial × axial extent) rectangular region by means of a 2D PIV system constituted by a double-cavity Nd:Yag pulsed laser and a Dantec High Sense Mk II digital camera. This has resulted in 6000 instantaneous distributions of 44×61 values of v_a and v_r, the axial and radial velocity components respectively. v_θ , the tangential one, has not been measured. The flow has been seeded by means of a fog generator and measurements have been taken at Ω = 2500 rev/min and at four operating points: $\psi = 0.0126$ (maximum BS width, approximating free-discharge conditions FD), 0.0488, 0.0993 (DP), and 0.1142.

The ensemble average technique, see Canepa et al. (2018) has been employed to extract the unresolved unsteadiness, i.e. that part of the flow unsteadiness not related to the blade passage periodicity. In rotating machinery, it cumulates both small-scale turbulence and non-periodic large-scale flow structures such as the ones released from the gap. In the present case, it is evaluated by means of the quantity $\widetilde{Tu}$, which is called turbulence intensity for the sake of simplicity; it is based

on the rms of the non-periodic part of the velocity fluctuations ($\widetilde{\overline{v_\theta'^2}}$ is missing since the PIV system did not allow to measure v_θ):

$$\widetilde{\overline{Tu}} = \frac{\sqrt{\frac{\left(\widetilde{\overline{v_a'^2}} + \widetilde{\overline{v_r'^2}}\right)}{2}}}{u_{tip}} \tag{4}$$

In a study of the leakage flow turbulence, the lack of information about $\widetilde{\overline{v_\theta'^2}}$ would constitute an important drawback, but it does not impair the conclusions of the present work, as it is aimed at finding a qualitative correlation between flow pattern and noise radiation.

EXPERIMENTAL RESULTS

Previous work

Some of the results of Canepa et al. (2018) are shortly summarized here, as they constitute the basis for the present work. Measurements were taken at Ω = 2400 and 3000 rev/min at $\psi = \psi_{DP}$; opposite to the present study, the investigated domain size was 95 mm × 70 mm (radial × axial extent).

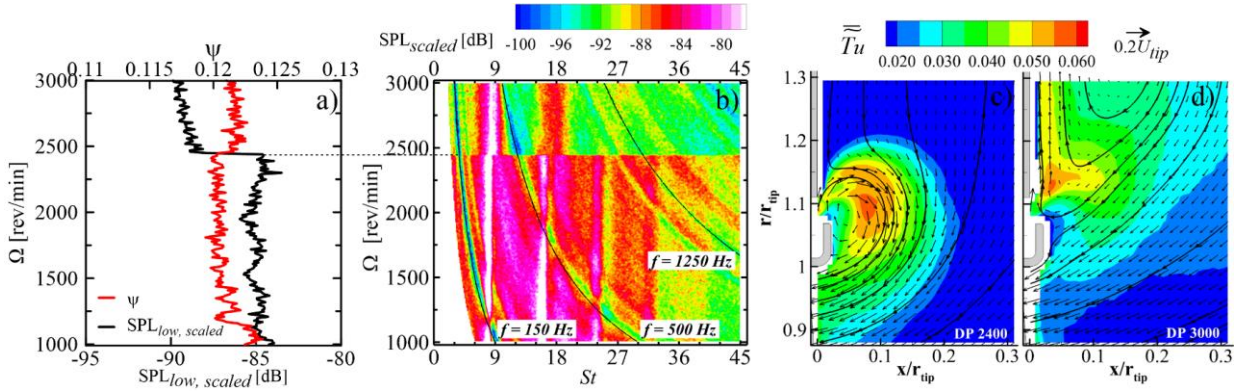

Figure 2: Measurements on a plastic rotor. a) $SPL_{low,scaled}$ and ψ during a speed ramp. b) SPL spectrogram during a speed ramp. c) Time-mean velocity field at 2400 rev/min. d) Time-mean velocity field at 3000 rev/min. (Partly taken from Canepa et al. (2018).)

During the acoustic measurements, Δp was acquired and resulted proportional to Ω^2, which indicated that similarity was apparently respected. ψ has been recently computed; its trend is reported versus Ω in Fig. 2a. $\psi \cong \psi_{DP} = 0.098$ in the range $\Omega \cong 1500 \div 2450$ rev/min, but below 1500 rev/min ψ is slightly decreasing and above 2450 rev/min a sudden increase of less than 2% takes place. The former variation may be caused by low-*Re* effects but it is of minor interest as the rotor is usually operated at higher Ω. The latter variation is within the typical uncertainties for such pressure rise measurements but should not be neglected as it is not random; this becomes apparent observing the trend of $SPL_{low,scaled}$, also reported in Fig. 2a. The slight fluctuations within the whole speed ramp, likely due to acoustic propagation effects, may be neglected, but the sudden decrease of about 4 dB that takes place at $\Omega \cong 2450$ rev/min is unexpected and cannot be explained based on common knowledge on fan noise. Such a behavior is related to the step in the SPL spectrogram of Fig. 2b, which reports the measured SPL spectrum computed in proportional bands with $\Delta St = 0.2$, $f_{min,n} = (n-1/2)\Delta St\Omega/60$, and $f_{max,n} = (n+1/2)\Delta St\Omega/60$ and then scaled according to Eq. (1). Valleys aligned along hyperbolas are due to propagation effects and may be neglected as aerodynamic issues are concerned here. The crests at subharmonic frequencies ($St \cong 8.4$, 17, 24, 32) are related to the leakage flow. Their height should be nearly independent from Ω, provided that a suitable α value has been employed in the scaling, see Canepa et al. (2017). The abrupt SPL decrease at $\Omega = \Omega_{step} \cong 2450$

rev/min indicates that a sudden modification in the flow pattern must take place. This is confirmed by the time-mean vector plots shown in Fig. 1, which are related to Ω values below and above 2450 rev/min, i.e. 2400 rev/min and 3000 rev/min. In the former case, a recirculation bubble is attached to the rotor ring, and the path followed by the large-scale structures released from the gap and reingested by the rotor is shorter than in the latter case, where a broad recirculation zone is present and a stronger decay of the turbulent structures is expected. Hence, the observed ψ variation, though small, is related to a dramatic modification in the leakage flow pattern and related noise. Measurements of the axial position of the ring showed that the combined effect of centrifugal force and blade loading results in a ring displacement in the forward direction: when stationary, the rotor is flush mounted, while it juts out of 3 mm and 4.2 mm at Ω = 2400 rev/min and 3000 rev/min, respectively. Further acoustic tests showed a cross dependence of Ω_{step} on both ψ and Ω. This indicated that the broad recirculation zone is typical of high ψ values, but it did not clarify whether it is characteristic of a rotor jutting out of the mounting panel.

Preliminary considerations on the acoustic measurements

ψ has been systematically computed and some of the trends related to speed ramps measurements are plotted in Fig. 3a (each case is identified by means of the corresponding average ψ value). Below 1800 rev/min, ψ increases or decreases with a maximum variation smaller than 5% of ψ_{DP}. Above 1800 rev/min, ψ is almost constant, with maximum variations smaller than 2% of ψ_{DP}, a value which compares to the typical accuracy of such a kind of pressure measurements. Likely, the ψ variations are due to a slight departure of the pressure drop through the BS from the assumed quadratic behaviour or, possibly, to low-*Re* effects. However, aerodynamic similarity is acceptably respected above 1800 rev/min, as, opposite to previous results, no abrupt steps are present.

The constant-Ω SPL spectra provide a first indication of the effect of the operating point on the radiated noise. Both original and filtered spectra related to Ω = 2500 rev/min are reported in Fig. 3b. The already mentioned propagation effects may be identified in the plot of the propagation function *G*(*f*), see Fig. 3c. The filtered spectra have smoother trends and show the interesting aspects more clearly. Namely, the subharmonic, narrowband humps due to the leakage flow, which are present in all of the cases, e.g. see Canepa et al. (2016a) or Piellard et al. (2014). Due to the leakage flow prerotation, their characteristic *St* values are smaller than the ones of the BPF harmonics (*St* = 9, 18, 27, etc.). As the frequency of the *i*-th BPF harmonic equals $i\,\Omega/60$, the non-dimensional frequency shift of a hump from BPF harmonics is given by

$$\Delta St_i = \frac{60\Delta f_i}{\Omega} \cong i\,\frac{v_\vartheta}{r\Omega} \tag{5}$$

where v_ϑ is the tangential component of the absolute velocity at the radial location *r* where the leakage flow is ingested by the blade, e.g. see Piellard et al. (2014). The low-frequency humps increase with ψ is the cause for the SPL_{low} growth. Such a behaviour is expected as the leakage mass flow increases with ψ also; however, the humps shape and peak *St* also vary and this may be due to a modification in the flow pattern. The behavior of the high-frequency part of the SPL spectrum is related to the boundary layer turbulence, and determines the SPL_{high} trend. The major contribution to SPL_{high} is provided by the broad hump between 5 and 10 kHz. It could be due to a feedback of the vortex shedding from the blade trailing edge on the boundary layer transition, a feature already observed by Henner et al. (2015). This explanation is consistent with the hump decrease and eventual disappearance as ψ increases, since the adverse pressure gradient on the blade suction side increases with ψ, likely making the boundary layer transition less sensitive to other perturbations.

Effect of the operating conditions on the radiated noise

In order to obtain quantitative information on the radiated noise, the acoustic measurements have been taken at Ω =2500, 3200, and 3900 rev/min. Then, SPL_{low}, SPL_{high}, and the OASPL have been

computed employing the original spectra, as propagation effects are less important when the SPL is computed on broad frequency ranges on which $G(f)$ oscillations compensate, see the plot of Fig. 3c.

First, SPL_{low}, SPL_{high}, and OASPL related to $\Omega = 3200$ rev/min are compared, see Fig. 4a. SPL_{low}, which is representative of the leakage noise, is always larger than SPL_{high}, which is related to the boundary layer noise. At low ψ, SPL_{high} causes a 1.5 dB difference between OASPL and SPL_{low}, while above $\psi \cong 0.04$ its contribution is negligible and OASPL $\cong SPL_{low}$; this shows that SPL_{low} provides the major contribution to the radiated acoustic power, thus confirming the importance of the leakage flow noise. Then, the dependence on Ω is considered. To this aim, SPL_{low}, SPL_{high}, and OASPL have been scaled according to Eq. (1), see Figs. 4b, 4c, 4d. $\alpha = 1$ has been employed as it has shown the best collapse of the $SPL_{low,scaled}$ curves below $\psi \cong 0.09$. For larger ψ values, a higher α (e.g. $\alpha = 1.4$) would be required. On the contrary, a smaller α (e.g. $\alpha = 0.5$) would result in a better

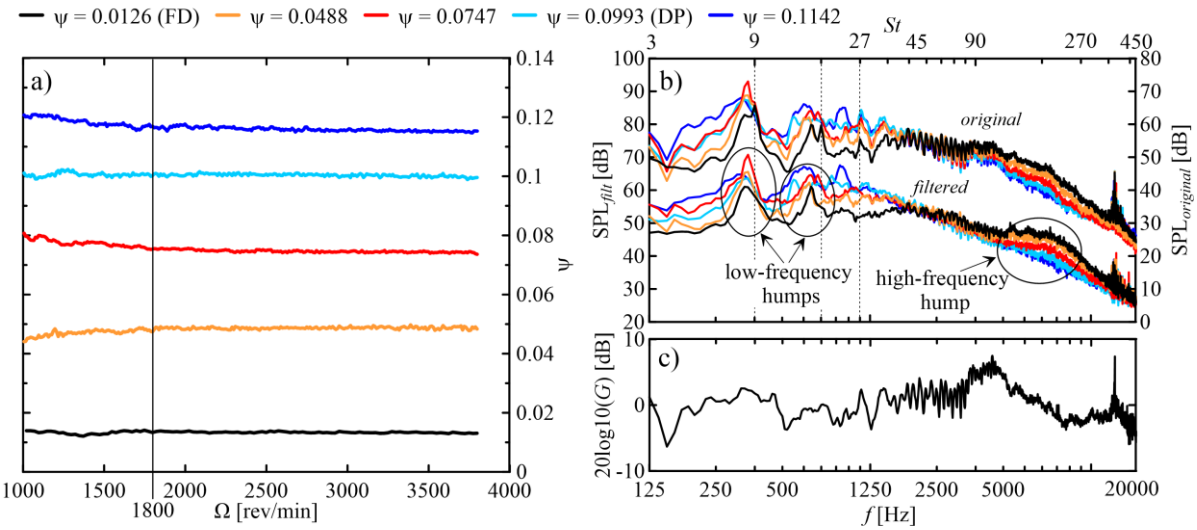

Figure 3: Acoustic measurements at fixed BS width. a) ψ trend during different speed ramps. b) Original and filtered SPL spectra at Ω = 2500 rev/min. c) Propagation function.

collapse of the SPL_{high} curves, but important discrepancies would remain. In fact, α grows with the coherence of the flow structures causing the noise and, hence, it may vary with both ψ and St, see Canepa et al. (2017). Thus, as noise is generated by a complicated flow, scaling the SPL with a unique α value is only qualitatively acceptable.

The three $SPL_{high,scaled}$ curves have similar trends, but show a spread between 1 and 4 dB which decreases with ψ, a Re dependence of the boundary layer transition could contribute to such discrepancies. Below $\psi \cong 0.085$, $SPL_{high,scaled}$ is always decreasing, then a minimum follows whose width depends on Ω, and, above $\psi \cong 0.11$, it is always increasing. Discrepancies between the three $SPL_{low,scaled}$ curves are limited to less than 2 dB and the trends are similar. As expected, $SPL_{low,scaled}$ increases with ψ since the leakage flow rate increases with ψ also, but, peculiarly, its trend is not monotonic, as the growth is interrupted by a sudden decrease at $\psi \cong 0.04 \div 0.045$ and by a further, smoother decrease between $\psi \cong 0.075 \div 0.0873$. Such a behavior is qualitatively independent from Ω. Although the maximum decrease is of a few dB only, these ψ values are characteristic ones, since important flow pattern modifications may be related to them.

In order to deepen the Ω dependence of SPL_{low}, the low-frequency part of $SPL_{filt,scaled}$ has been plotted as a function of both St and ψ in the spectrogram of Fig. 5a, which is related to $\Omega = 3200$ rev/min. Indeed, the spectrograms related to 2500 and 3900 rev/min (not reported for the sake of space) show crests, valleys, and plateaus with similar shapes. This qualitative independence from Ω confirms that aeroacoustic similarity is qualitatively respected also. Hence, opposite to the case of the plastic rotor, see Fig. 2c and 2d, no sudden flow pattern modifications take place as Ω grows and the analysis may be continued with reference to one Ω value only.

Below $St = 45$, the SPL spectrum shows the highest values and strongly grows with ψ, yielding the observed increase of SPL_{low}. A number of vertical crests are present in the plot, but the ones below $St = 9$, 18, 27, and 36 are the most important ones, as they are generated by the interaction of the rotor blades with the prerotating large-scale flow structures; the higher-St crests are harmonics of the first one. They correspond to the narrowband humps observed in the constant-Ω spectra. According to Eq. (5), in a first approximation, the lower the characteristic St, the higher the prerotation. Furthermore, a narrow, high crest indicates that the flow structures have a high coherence and viceversa, see the analysis of Majumbdar and Peake (1998) on the ingestion of large-scale turbulence by propellers.

Up to $\psi \cong 0.075$, the crests widen, their characteristic St seems slightly decreasing, and their height gradually increases; this agrees with the SPL_{low} trend. The SPL_{low} minimum which takes place at $\psi \cong 0.04$ seems related to the local maxima between $St = 36$ and 42 in the spectrogram. Between $\psi \cong 0.075$ and $\psi \cong 0.087$, a horizontal, lower-level band is present which extends up to $St = 36$; it should

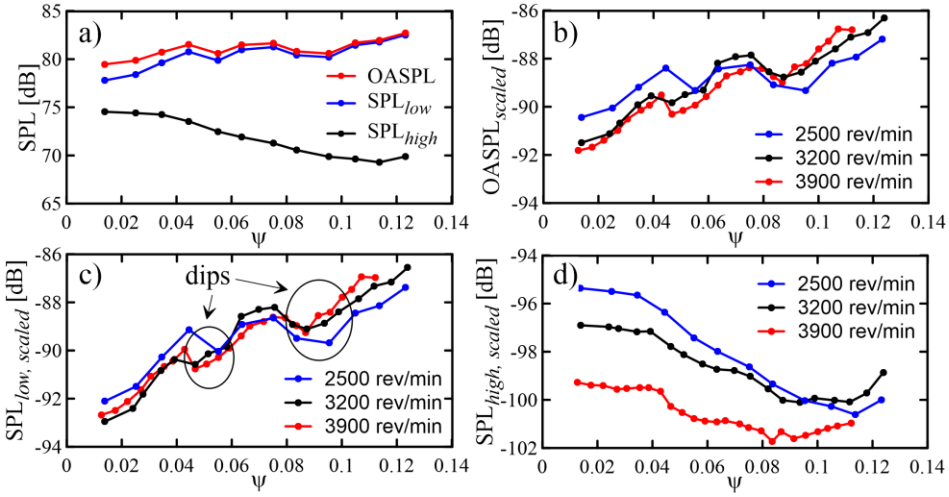

Figure 4: SPL in different frequency ranges. a) SPL_{low}, SPL_{high} and OASPL at Ω = 3200 rev/min. b) $OASPL_{scaled}$ at Ω = 2500, 3200 and 3900 rev/min. c) $SPL_{low,scaled}$ at Ω = 2500, 3200 and 3900 rev/min. d) $SPL_{high,scaled}$ at Ω = 2500, 3200 and 3900 rev/min.

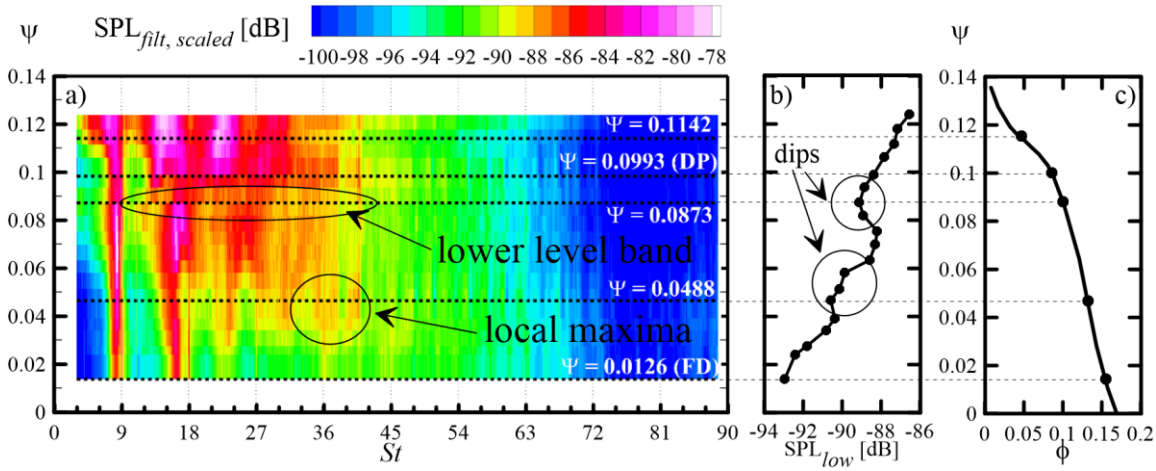

Figure 5: Acoustic analysis at Ω = *const.* a) spectrogram at 3200 rev/min. b) $SPL_{low,scaled}$ at 3200 rev/min. c) non-dimensionalized characteristic curve of the rotor.

be related to the second minimum of SPL_{low}. Then, as ψ grows beyond about 0.09, the first crest gradually increases, broadens, and shifts towards lower St. On the contrary, the other crests apparently merge in a plateau extending from $St \cong 12$ to $St \cong 37$; as ψ further grows, two very high and broad crests appear whose characteristic St has clearly decreased compared to the values at $\psi < 0.075$. Possibly, a change in the flow pattern takes place across $\psi \cong 0.09$, e.g. stronger flow structures with

a higher degree of prerotation substitute the ones present at lower ψ. A confirmation of such a hypothesis will be sought in the flow features.

Relation between radiated noise and flow pattern

At most, the collapse of the $SPL_{low,scaled}$ curves of Fig. 4c may be considered fair, suggesting that aeroacoustic similarity is not fully respected while Ω varies; however, it is important to verify whether this depends on the leakage noise. Hence, the SPL spectrum in the low- to medium-frequency range ($St < 45$) has been plotted versus St and Ω in Fig. 6. The spectrograms reporting the original SPL scaled with $\alpha = 1$ (1st row) are strongly distorted by propagation effects, which complicate analyzing the plots. Then, SPL_{scaled} has been filtered (2nd row); although some valleys aligned along hyperbolas are still present at low Ω in all of the plots, the main features of the noise generating mechanism may be more clearly observed. Some tonal components likely due to large-scale turbulence ingestion are present at the lowest ψ. They may be identified as sharp, constant-St crests at St = 9, 18, 27, see Canepa et al. (2016b), that do not affect the main features of the spectrograms, and, hence, may be neglected in the present analysis. The subharmonic crests are the most interesting aspect of the spectrograms, as the narrowband humps observed in the SPL_{filt} spectra of Fig. 3b are constant-Ω cuts of them. They constitute the major contribution to SPL_{low} and are present at all ψ, confirming that the leakage noise is always important for the present rotor. As Ω varies, their characteristic St values are basically constant and their height variation is gradual. Opposite to the previous work, no abrupt variations are present, thus confirming that the flow pattern is basically independent of Ω although the employed α is not the exact one.

At $\psi = 0.0126$, only the first three crests seem relevant. The level of all of them decreases with Ω, indicating that the α value employed in the scaling is too large. At the higher ψ, both height and width of the crests increase with Ω, and a fourth crest arises between St = 27 and 36. If the aeroacoustic similarity were fully respected and the exact α value were employed, characteristic St value and height of such crests would be independent of Ω. The slight ψ variations during the Ω ramps and some residual propagation effects likely reflect on the trend of the crests, thus preventing them from strictly respecting aeroacustic similarity. Nevertheless, the main features of the spectrograms are qualitatively independent of Ω, showing that, opposite to the case of the plastic rotor studied in Canepa et al. (2017, 2018, and 2019), no important flow pattern modifications take place as Ω grows. Hence, it may be concluded that, for the present rotor, aerodynamic measurements taken at a single Ω value are sufficient to characterize the leakage flow pattern related to a given ψ.

Such a kind of measurements have been taken in the meridional plane region shown in Fig. 1, at Ω = 2500 rev/min and ψ = 0.0126 (FD), 0.0488, 0.0993 (DP), 0.1142. Different aerodynamic quantities are reported in Fig. 6: time-mean vector plots with the $\widetilde{\overline{Tu}}$ contours (3rd row) and instantaneous vector plots (4th row). The latter ones are not representative of the most statistically frequent pattern; rather, they have been chosen since show a strong instantaneous leakage flow and help explain some flow features. Extracting further information about large-scale flow structures would require an analysis based on suitable techniques. To this aim, Canepa et al. (2019) successfully applied the proper orthogonal decomposition algorithm presented in Simoni et al (2017) and Lengani et al. (2017) to the leakage flow in the plastic rotor of Fig. 1e. However, although single instantaneous flow fields are not statistically relevant, Canepa et al. (2018) showed that they may help identify interesting features of the unsteady flow.

Despite the subharmonic narrowband humps in the SPL spectra, at low ψ (0.0126), the leakage flow may not be easily detected in the time-mean vector plots as the flow is centripetal and no velocity component pointing upstream of the rotor may be detected. However, in front of the ring, a higher-$\widetilde{\overline{Tu}}$ area is present and the instantaneous vector plot shows that, in the lower part of the gap, the flow points upstream. All this is consistent with the presence of a weak leakage flow.

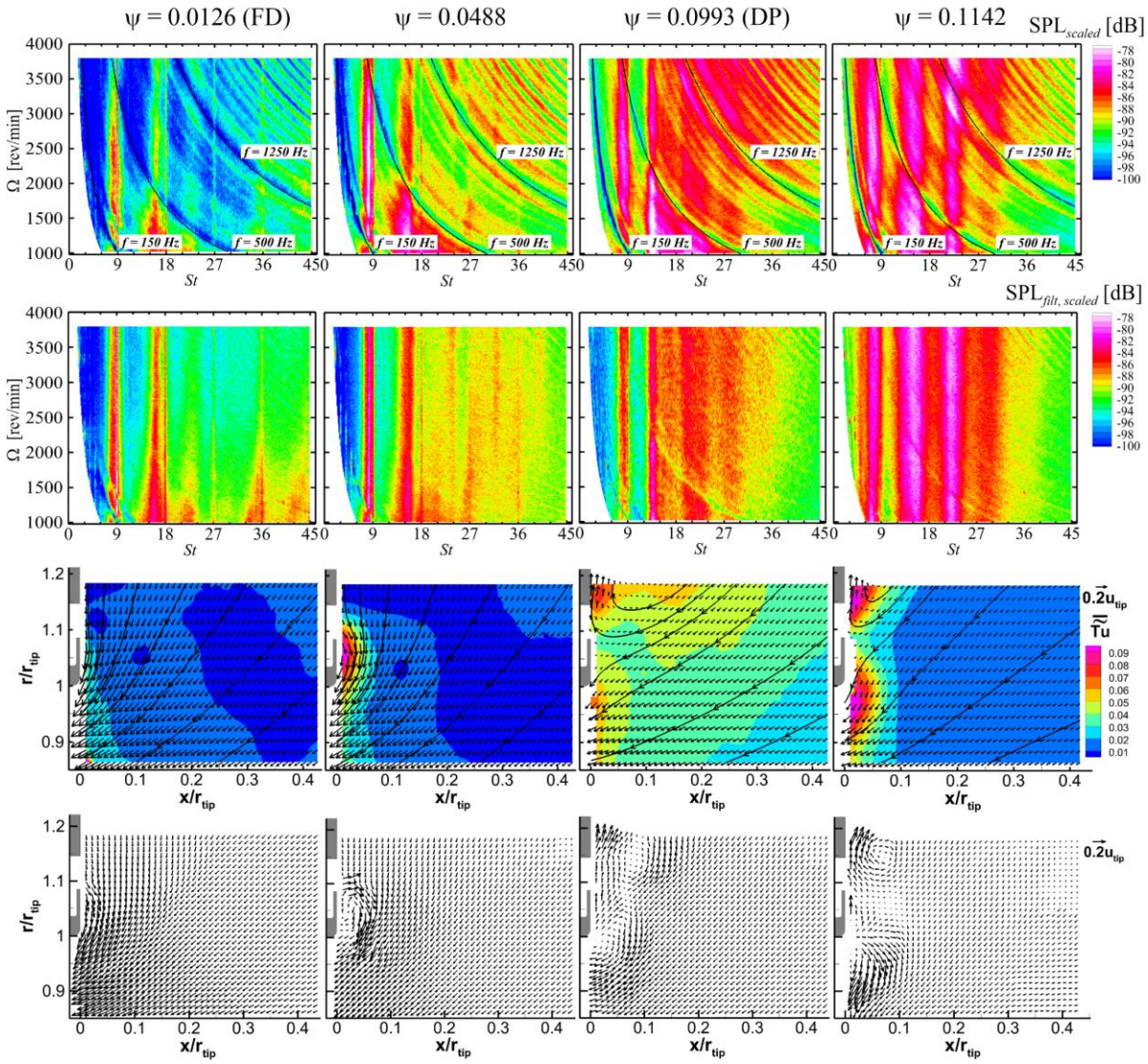

Figure 6: Measurements taken at $\psi = const.$ From top to bottom: spectrograms of SPL_{scaled} and of $SPL_{filt,scaled}$ during speed ramps, and time-mean and instantaneous flow fields at Ω = 2500 rev/min. From left to right: ψ = 0.0126, 0.0488, 0.0993, 0.1142.

At $\psi = 0.0488$, the time-mean flow is still centripetal but shows a clear deflection in front of the gap and a high $\overline{\widetilde{Tu}}$ in front of the ring; these are evidences of the presence of the leakage flow. The instantaneous flow field shows that, in front of the gap, some velocity vectors point upstream, clearly confirming the leakage flow presence. Furthermore, a recirculation bubble is present in front of the ring, as in the case of the plastic rotor at Ω = 2400 rev/min, see Fig. 2c.

At $\psi = 0.0993$ and 0.1142, the time-mean flow pattern is completely different: the leakage flow streams radially outwards along the panel and forms a wide recirculation zone, as in the case of plastic rotor at Ω = 3000 rev/min, see Fig. 2d. This shows that such a flow pattern is present also in case of stiff, flush mounted rotor, i.e. it seems characteristic of the high-ψ operation of a rotor mounted on a flat panel rather than of the rotor jutting out of it. However, the high-$\overline{\widetilde{Tu}}$ zone in front of the blade tip and of the lower part of the ring is absent in the plastic rotor case and may not be explained based on turbulence convection from the gap towards the rotor entrance. In fact, the instantaneous vector plots show that a reverse flow area is sometimes present at the blade tip. Obviously, the presence of such a separation constitutes an undesired total pressure loss and reduces the rotor efficiency. Such a loss does not likely affect the rotor performance, as it could consist in a kinetic energy loss compensated by a larger static pressure rise, which, for such fans, constitutes the design target. Statistically, such a flow pattern is not so frequent, and, apparently, it does not affect the time-mean velocity field;

however, it constitutes an important reason of unsteadiness which results in the observed high $\widetilde{\overline{Tu}}$ zone. At $\psi = 0.1142$, such a separated flow is stronger than at $\psi = 0.0993$. Furthermore, it must have an important prerotation as it comes from the rotor, and, eventually, is partly reingested at lower radii. Despite the different origin, such a recirculating flow has likely characteristics similar to the leakage flow ones (positive swirl and presence of unsteady large-scale structures). This could be a further cause of subharmonic narrowband humps in the SPL spectrum. This hypothesis is consistent with the modifications in the SPL spectrum across $\psi \cong 0.09$, see Fig. 5a, and also suggests an explanation for it. At $\psi = 0.0993$, only the first subharmonic crest may be detected, as the other ones seem to merge in a rather flat plateau, see also the constant-Ω spectra of Fig. 3b. At $\psi < 0.09$, the 2nd, 3rd, and 4th crests are located at higher *St* than they are at $\psi > 0.10$. A possible explanation for this is that, in the former case, the main contribution to the noise is due to the leakage flow, while, in the latter case, the reverse flow in the blade tip region could overwhelm the leakage flow, thus providing the major contribution to the noise generation. The lower characteristic *St* values could be ascribed to a stronger prerotation, due to the fact that the separated flow directly comes from the blade region and also follows a shorter path before being reingested. Subharmonic humps in the SPL spectrum of rotors without ring have been reported by Zhu et al. (2018), who ascribed them to the leakage flow between blade tip and stationary shroud, a reverse flow which presents some analogies with present one. At $\psi = 0.0993$, the two flows could provide similar contributions to the noise generation, resulting in the observed plateau. The vortical structures which may be observed in the upper part of the plot are due to the shear layer which forms between the main flow, which points towards the rotor, and the leakage flow, which is restrained between the panel and the recirculation zone. Obviously, though realistic, such explanations require further confirmation.

CONCLUSIONS

The leakage flow and related noise in low-speed fans with rotating shroud have been experimentally studied at different operating conditions and rotational speeds. The present work has shown that, when the fan is operated during speed ramps, the flow basically respects similarity despite some variations in the pressure rise coefficient. This allows to take measurements at variable rotational speed, which is essential for acoustic measurements. The observed variations may result in slight modifications in the SPL spectra, but the flow pattern is basically independent from the rotational speed, since the studied rotor is stiff and low-Reynolds number effects are negligible. This indicates that the aeroacoustic similarity is basically respected for a stiff rotor; on the contrary it may not be the case for plastic rotors which usually deform during operation, possibly resulting in dramatic modifications of flow pattern and SPL spectrum.

The leakage flow always provides the main contribution to the SPL spectrum, and its pattern depends on the operating conditions and not on the rotational speed. At low blade loading, the leakage flow is restrained close to the rotor ring, while, at high loading, it flows radially outward along the mounting panel forming a broad recirculation zone. In the latter condition, an unsteady flow separation in the blade tip region is likely present, which could result in the appearance of subharmonic narrowband humps in the spectrum, a feature typical of the leakage noise. It likely mixes with the leakage flow resulting in a non-monotonic trend of the SPL with the loading. This confirms that the properties of the noise in the low-frequency range are very complicated, as it not only depends on the leakage flow, that is on the pressure rise through the rotor and on the gap geometry, but also on the aerodynamic behaviour of the blade within the whole range of operation.

ACKNOWLEDGEMENTS

The authors kindly acknowledge Johnson Electric Asti srl for having provided the tested rotor.

REFERENCES

Bongiovì, A., Cattanei, A., (2011). *Spectral decomposition of the aerodynamic noise generated by rotating sources*. J. Sound Vib. 330, 136–152.

Canepa, E., Cattanei, A., Mazzocut Zecchin, F., (2015). *Installation effects on the tonal noise generated by axial flow fans*. J. Sound Vib. 340 167–189.

Canepa, E., Cattanei, A., Mazzocut Zecchin, F., Milanese, G., Parodi, D., (2016a). *An experimental investigation on the tip leakage noise in axial-flow fans with rotating shroud*. J. Sound Vib. 375, 115–131.

Canepa, E., Cattanei, A., Mazzocut Zecchin, F., (2016b). *Analysis of tonal noise generating mechanisms in low-speed axial-flow fans.* J. Thermal Sci. 25(4), 302–311.

Canepa, E., Cattanei, A., Mazzocut Zecchin, F., (2017). *Scaling properties of the aerodynamic noise generated by low-speed fans.* J. Sound Vib. 408, 291–313.

Canepa, E., Cattanei, A., Jafelice, F., Mazzocut Zecchin, F., Parodi, D., (2018). *Effect of rotor deformation and blade loading on the leakage noise in low-speed axial fans*. J. Sound Vib. 433, 99–123.

Canepa, E., Cattanei, A., Mazzocut Zecchin, F., Parodi, D., (2019). *Large-scale unsteady flow structures in the leakage flow of a low-speed axial fan with rotating shroud*. Exp. Therm. Fluid Sci., 102, 1–19.

Fukano, T., Takamatsu, Y., Kodama, Y., (1986). *The effects of tip clearance on the noise of low pressure axial and mixed flow fans*. J. Sound Vib. 105 (2) 291–308.

Fukano, T., Jang, C.-M., (2004). *Tip clearance noise of axial flow fans operating at design and off-design condition*, J. Sound Vib. 275 1027–1050.

Henner, M., Franquelin, F., Demory, B., Beddadi, Y., Roland, C., Serran, A., (2015). *Hump-shaped broadband noise on a fan at off-design conditions*. Fan 2015, Lyon, France, April 2015.

ISO 10302, (1996), Acoustics-Method for the measurement of airborne noise emitted by small air-moving devices.

Lengani D., Simoni D., Ubaldi M., Zunino P., Bertini F., (2017). *Analysis of the Reynolds stress component production in a laminar separation bubble*, Int. J. Heat Fluid Flows 64, 112–119.

Longhouse, R., (1978). *Control of tip-vortex noise of axial flow fans by rotating shrouds*. J. Sound Vib. 58 (2) 201–214.

Magne, S., Moreau, S., Berry, A., (2015). *Subharmonic tonal noise from backflow vortices radiated by a low-speed ring fan in uniform inlet flow*. J. Acoust. Soc. Am. 137 (1) 228–237.

Majumdar, S. J., Peake, N., (1998). *Noise generation by the interaction between ingested turbulence and a rotating fan*. J. Fluid Mech. 359 181–216.

Moreau, S., Sanjose, M., (2016). *Sub-harmonic broadband humps and tip noise in low-speed ring fans.* J. Acoust. Soc. Am. 139 (1) 118–127.

Na, G.-D., Kameier, F., Springer, N., Mauß, M., Paschereit, C.O., (2017). *URANS simulations and experimental investigations on unsteady aerodynamic effects in the blade tip region of a shrouded fan configuration*. ASME Paper GT2017-63680, Proc. of the ASME Turbo Expo, Charlotte, USA.

Neise, W., Barsikow, B., (1982). *Acoustic similarity laws for fans.* J. Eng. Ind. Trans. ASME 104 (2), 162–168.

Piellard, M., Coutty, B., Le Goff, V., Vidal, V., Pérot, F., (2014). *Direct aeroacoustics simulation of automotive engine cooling fan system: Effect of upstream geometry on broadband noise*. 20th AIAA/CEAS Aeroacoustics Conference, Atlanta, USA.

Simoni D., Lengani D., Ubaldi M., Zunino P., Dellacasagrande M., (2017). *Inspection of the dynamic properties of laminar separation bubbles: free-stream turbulence intensity effects for different Reynolds numbers*, Exp. Fluids 58 (6) 66.

Zenger, F.J., Renz, A., Becher, M., Becker, S., (2016). *Experimental investigation of the noise emission of axial fans under distorted inflow conditions*. J. Sound Vib. 383 124–145.

Zhu, T., Lallier-Daniels, D., Sanjose, M., Moreau, S., Carolus, T., (2018). *Rotating coherent flow structures as a source for narrowband tip clearance noise from axial fans*. J. Sound Vib. 417 (2018) 198–215.